Tetrahedron 65 (2009) 10565–10572

Contents lists available at ScienceDirect

Tetrahedron

journal homepage: www.elsevier.com/locate/tet

2,6-*Cyclo*-xenicanes from the brown algae *Dilophus fasciola* and *Dilophus spiralis*

Efstathia Ioannou [a], Maria Zervou [b], Amel Ismail [c], Leila Ktari [c], Constantinos Vagias [a], Vassilios Roussis [a,*]

[a] *Department of Pharmacognosy and Chemistry of Natural Products, School of Pharmacy, University of Athens, Panepistimiopolis Zografou, Athens 15771, Greece*
[b] *Institute of Organic and Pharmaceutical Chemistry, National Hellenic Research Foundation, Vas. Constantinou 48, Athens 11635, Greece*
[c] *National Institute of Marine Sciences and Technologies (INSTM), Laboratory of Biodiversity and Marine Biotechnology, 28 rue du 2 Mars 1934, Salammbô 2025, Tunisia*

ARTICLE INFO

Article history:
Received 4 August 2009
Received in revised form
5 October 2009
Accepted 22 October 2009
Available online 25 October 2009

Keywords:
Dilophus fasciola
Dilophus spiralis
2,6-*cyclo*-Xenicanes
Molecular modelling

ABSTRACT

Seven new diterpenes, featuring the rare 2,6-*cyclo*-xenicane skeleton, along with eleven previously reported metabolites were isolated from the organic extracts of the brown algae *Dilophus fasciola* and *Dilophus spiralis*. The structure elucidation of the isolated natural products was based on detailed analyses of their spectroscopic data (NMR, MS, IR, UV), whereas the assignment of their relative configurations was assisted by molecular modelling studies.

© 2009 Elsevier Ltd. All rights reserved.

1. Introduction

Seaweeds belonging to the family Dictyotaceae are regarded as a prolific source of normal and mixed biosynthesis terpenoid metabolites, often exhibiting cytotoxic, antibacterial, algicidal, antifeedant and ichthyotoxic activities.[1,2] Brown algae of the genera *Dictyota* and *Dilophus* have been shown to produce mainly sesquiterpenes and diterpenes, featuring a diverse array of carbon skeletons.

In a preliminary screening of a number of algal extracts, the organic extract of *Dilophus fasciola* (*syn. mediterraneus*) displayed significant antifouling activity against a panel of marine fouling bacteria, whereas the dichloromethane extract of *Dilophus spiralis* (*syn. ligulatus*) exhibited noteworthy levels of cytotoxicity. Furthermore, their interesting chemical profiles, in conjunction with the limited information on the chemical composition of both species, prompted us to undertake a thorough investigation towards the isolation of their bioactive metabolites.

In this report, we describe the isolation and structure elucidation of the seven new minor metabolites **1**–**7**. The new natural products feature the rare 2,6-*cyclo*-xenicane skeleton, previously reported only once, without determination of the relative stereochemistry of the isolated compounds, from an Australian collection of the brown alga *Dictyota dichotoma*.[3] The relative configuration of the stereogenic centre at C-13 for compounds **2**–**5**, which was not possible to be assigned using NMR spectroscopic techniques, was proposed on the basis of the results obtained from extensive molecular modelling studies.

2. Results and discussion

A series of chromatographic separations of the CH_2Cl_2 and MeOH extracts of *D. spiralis*, collected in Greece, resulted in the isolation of one new 2,6-*cyclo*-xenicane (**1**) and seven previously reported metabolites, which were identified as acetyldictyolal,[4] neodictyolactone,[5] pachylactone,[6] obscuronatin,[7–9] *trans*-phytol,[10,11] fucosterol,[12,13] and all-*E*-(3*S*,5*R*,6*S*,3′*S*,5′*R*,6′*R*)-fucoxanthin[14,15] by comparison of their spectroscopic and physical characteristics with those reported in the literature. In a similar manner, the CH_2Cl_2/MeOH extract of *D. fasciola*, collected in Tunisia, was subjected to repetitive chromatographic fractionations and HPLC purifications to provide six new 2,6-*cyclo*-xenicanes (**2**–**7**) and seven previously described compounds, which were identified as acetyldictyolal,[4] neodictyolactone,[5] dictyol C,[16] dictyol E,[16] sanadaol,[17] 18-hydroxy-2,7-dolabelladiene,[18] and fucosterol[12,13] by comparison of their spectroscopic and physical characteristics with those reported in the literature.

Compound **1**, obtained as a colourless oil, displayed an ion peak at *m*/*z* 303.2340 (HR-FABMS), corresponding to $C_{20}H_{31}O_2$ and consistent for $[M+H]^+$. The ^{13}C NMR spectrum and DEPT experiments exhibited 20 signals, corresponding to four methyl, six methylene, six methine, and four quaternary carbon atoms. Among

* Corresponding author. Tel./fax: +30 210 7274592.
E-mail address: roussis@pharm.uoa.gr (V. Roussis).

0040-4020/$ – see front matter © 2009 Elsevier Ltd. All rights reserved.
doi:10.1016/j.tet.2009.10.081

them, evident were two aldehyde carbonyls (δ 193.5 and 203.8), as well as two tertiary and two quaternary olefinic carbons (δ 124.7, 131.2, 144.0 and 152.2). The ^{1}H NMR spectrum of **1** indicated the presence of three methyls on quaternary carbons (δ 0.95, 1.55 and 1.63), one methyl on a tertiary carbon (δ 1.00), two olefinic methines (δ 5.02 and 6.94), and two aldehyde groups (δ 9.39 and 9.78). Since the two carbon–carbon double bonds and the two carbonyls accounted for four of the six degrees of unsaturation, **1** was assumed to be bicyclic. The presence of an aldehyde proton appearing as a singlet, in conjunction with the presence of an olefinic proton appearing as a triplet and resonating at lower fields (δ 6.94), indicated a disubstituted α,β-unsaturated aldehyde in the molecule and suggested that the olefinic proton was positioned at the β carbon, adjacent to a methylene. This hypothesis was further verified by the maximum absorption at λ_{max} 229.5 nm in the UV spectrum. Analysis of the 2D NMR spectra (HSQC, HMBC and COSY) of **1** assisted in the determination of its carbon skeleton (Tables 1 and 2, Fig. 1). Specifically, the HMBC correlations of C-1, C-2 and C-9 with H-19 and of C-2 and C-6 with H_2-7, in conjunction with the cross-peaks of H_2-7/H_2-8 and H_2-8/H-9 observed in the COSY spectrum identified the six-membered ring. The correlations of C-2 with H-3 and H_2-5 and of the latter with C-6, in combination with the cross-peaks of H-3/H_2-4 και H_2-4/H_2-5 concluded the assignment of the five-membered ring. Further correlations of C-1 and C-2 with H-18 and of C-2, C-5, C-6 and C-7 with H_3-20 placed the second aldehyde and the aliphatic methyl group appearing as a singlet at C-2 and C-6, respectively. The cross-peaks of H-10/H_2-11, H-10/H_3-17, H_2-11/H_2-12 and H_2-12/H-13, as well as the correlations of C-13 and C-14 with H_3-15 and H_3-16 displayed in the HMBC spectrum determined the structure of the side chain, while the correlations of C-11 and C-17 with both H-3 and H-10, despite the absence of a cross-peak between H-3 and H-10 in the COSY spectrum, fixed its position at C-3.

Table 2
^{13}C NMR spectroscopic data of compounds **1**–**5** in $CDCl_3$

C	**1**		**2**		**3**		**4**		**5**	
1	144.0	s	n.d.	s	146.6	s	n.d.	s	146.5	s
2	61.6	s	n.d.	s	62.7	s	61.7	s	61.5	s
3	54.2	d	53.1	d	53.3	d	53.3	d	53.5	d
4	22.7	t	23.1	t	23.2	t	22.2	t	22.2	t
5	36.4	t	30.6	t	30.6	t	34.9	t	34.9	t
6	45.3	s	n.d.	s	50.0	s	49.4	s	49.1	s
7	32.5	t	71.3	d	71.4	d	69.9	d	69.9	d
8	23.9	t	n.d.	t	31.3	t	32.7	t	32.5	t
9	152.2	d	147.9	d	148.0	d	148.5	d	148.6	d
10	32.2	d	31.9	d	32.0	d	31.6	d	31.5	d
11	38.5	t	35.6	t	35.5	t	35.1	t	35.1	t
12	26.0	t	34.5	t	34.6	t	34.5	t	34.4	t
13	124.7	d	67.1	d	67.0	d	67.1	d	67.0	d
14	131.2	s	n.d.	s	144.5	s	144.5	s	144.3	s
15	25.7	q	114.2	t	114.3	t	114.1	t	114.2	t
16	17.6	q	17.0	q	17.0	q	17.1	q	16.9	q
17	16.8	q	17.7	q	17.5	q	17.0	q	16.7	q
18	203.8	d	204.7	d	204.8	d	206.7	d	206.5	d
19	193.5	d	193.2	d	193.3	d	193.4	d	193.5	d
20	22.7	q	20.5	q	20.4	q	18.9	q	18.9	q

n.d.: not detected.

H-10 and H_3-17 were below the plane of the five-membered ring and thus defined the relative configuration at C-3 as *S**, which was further verified by the NOE enhancements of H-3/H-4β, H-3/H-7β, H-4α/H-18 and H-7α/H_3-20. The cross-peaks of H-4α/H_3-17 and H-10/H-19 observed in the NOESY spectrum, in conjunction with the lack of COSY correlation between H-3 and H-10, suggesting that the dihedral angle H-3–C-3–C-10–H-10 was approximately 90°, indicated that the relative configuration at C-10 was *R**. Therefore, compound **1** was assigned as (2*R**,3*S**,6*R**,10*R**)-2,6-*cyclo*-1(9),13-xenicadiene-18,19-dial.

Table 1
^{1}H NMR spectroscopic data of compounds **1**–**5** in $CDCl_3$

C		**1**		**2**		**3**		**4**		**5**
3		2.14 m		2.10 m		2.09 m		2.10 m		2.09 m
4	α	1.97 m	α	1.74 m	α	1.75 m	α	1.83 m	α	1.84 m
	β	1.75 m	β	1.70 m	β	1.71 m	β	1.66 m	β	1.65 m
5	α	1.59 m	α	1.59 m	α	1.60 m	α	1.49 m	α	1.47 m
	β	1.64 m	β	1.56 m	β	1.56 m	β	1.67 m	β	1.64 m
7	α	1.42 dt (13.8, 5.8)		3.84 dt (9.8, 5.7)		3.83 dt (9.8, 5.7)		3.77 dt (8.7, 4.5)		3.78 dt (8.7, 4.5)
	β	1.77 m								
8		2.38 m	α	2.68 dt (19.6, 5.7)	α	2.68 dt (19.5, 5.7)	α	2.57 dt (20.1, 4.5)	α	2.57 dt (20.1, 4.5)
			β	2.37 ddd (19.6, 9.8, 2.2)	β	2.37 ddd (19.5, 9.8, 2.2)	β	2.72 ddd (20.1, 4.5, 3.2)	β	2.72 ddd (20.1, 4.5, 3.2)
9		6.94 t (3.9)		6.73 dd (5.7, 2.2)		6.73 dd (5.7, 2.2)		6.83 dd (4.5, 3.2)		6.83 dd (4.5, 3.2)
10		2.11 m		2.58 m		2.57 m		2.52 m		2.53 m
11	a	1.18 m	a	1.39 m	a	1.36 m	a	1.34 m	a	1.32 m
	b	1.14 m	b	1.21 m	b	1.23 m	b	1.17 m	b	1.16 m
12	a	1.93 m		1.79 m	a	1.89 m		1.75 m	a	1.85 m
	b	1.85 m			b	1.76 m			b	1.72 m
13		5.02 t (7.2)		4.35 t (7.2)		4.35 t (7.3)		4.32 t (7.3)		4.32 t (7.2)
15		1.63 s	a	4.99 br s	a	5.00 br s	a	4.98 br s	a	4.99 br s
			b	4.86 br s	b	4.87 br s	b	4.85 br s	b	4.86 br s
16		1.55 s		1.77 s		1.77 s		1.77 s		1.77 s
17		1.00 d (6.6)		1.07 d (6.7)		1.07 d (6.8)		0.98 d (6.8)		0.98 d (6.8)
18		9.78 s		9.97 s		9.97 s		9.91 s		9.91 s
19		9.39 s		9.25 s		9.25 s		9.34 s		9.34 s
20		0.95 s		1.15 s		1.15 s		1.05 s		1.05 s
7-OH		—		1.55 m		1.55 m		3.43 m		3.43 m

The relative configuration of **1** was established by analysis of the key correlations displayed in the NOESY spectrum. In particular, the strong NOE interaction observed between H-18 and H_3-20 suggested the *cis* fusion of the two rings and determined the relative configuration at C-2 and C-6 as 2*R**,6*R**. NOE enhancements observed for H-10/H-18 and H_3-17/H-18 provided evidence that both

Compound **2**, isolated as a colourless oil, had the molecular formula of $C_{20}H_{30}O_4$, as deduced from the HR-FABMS data (*m*/*z* 334.2171 $[M]^+$). The fragment ions at *m*/*z* 317 $[M+H-H_2O]^+$ and 299 $[M+H-2H_2O]^+$ in the mass spectrum, as well as the absorption bands at 3358 and 3331 cm^{-1} in the IR spectrum indicated the presence of two hydroxy groups. The ^{1}H NMR spectrum of **2**

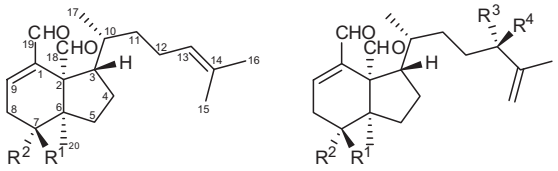

1 $R^1 = R^2 = H$
6 $R^1 = OH$, $R^2 = H$
7 $R^1 = H$, $R^2 = OH$

2 $R^1 = R^3 = OH$, $R^2 = R^4 = H$
3 $R^1 = R^4 = OH$, $R^2 = R^3 = H$
4 $R^1 = R^4 = H$, $R^2 = R^3 = OH$
5 $R^1 = R^3 = H$, $R^2 = R^4 = OH$

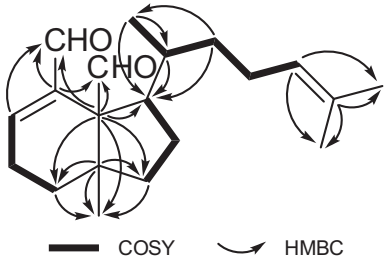

Figure 1. COSY and important HMBC correlations for compound **1**.

revealed the presence of two methyls on quaternary carbons (δ 1.15 and 1.77), one methyl on a tertiary carbon (δ 1.07), two oxygenated methines (δ 3.84 and 4.35), an exomethylene group (δ 4.86 and 4.99), an olefinic methine of a trisubstituted double bond (δ 6.73), and two aldehyde groups (δ 9.25 and 9.97). Analysis of the spectroscopic data of **2** (Tables 1 and 2) showed a high degree of similarity with metabolite **1**. In agreement with the molecular formula, it was clear that the difference was the replacement of the trisubstituted double bond in the side chain by a 1,1-disubstituted double bond and the presence of two hydroxy groups. The cross-peaks of H-7/H_2-8, in conjunction with the correlations of C-6 and C-7 with H_2-8 and H_3-20 observed in the HMBC spectrum, positioned the first hydroxy group at C-7, while the cross-peak of H_2-12/H-13 and the HMBC correlations of C-12, C-14, C-15 and C-16 with H-13 fixed the position of the second hydroxy group at C-13, thus identifying the planar structure of **2**.

Compound **3** was isolated by HPLC as a colourless oil, eluting 0.55 min after metabolite **2**. The HR-FABMS data (*m*/*z* 334.2163 $[M]^+$) suggested the same molecular formula as in **2** and the close resemblance of their spectroscopic data (Tables 1 and 2) indicated that **3** was a stereoisomer of the latter. The only distinct difference between the two compounds was that the methylene protons at C-12 resonated at δ 1.76 and 1.89 ppm in **3**, whereas in **2** they were magnetically equivalent, both resonating at δ 1.79 ppm.

The relative configuration of the chiral centres in compounds **2** and **3** was assigned on the basis of the key correlations observed in their respective NOESY spectra. In accordance with metabolite **1**, the relative configuration at C-2, C-3, C-6 and C-10 was determined as 2*R**,3*S**,6*R**,10*R** due to the NOE cross-peaks of H-3/H-4β, H-4α/H_3-17, H-10/H-18, H_3-17/H-18 and H-18/H_3-20, while the relative configuration at C-7 was assigned as *S** based on the NOE enhancements of H-7/H-8α, H-7/H_3-20 and H-5β/H-8β. Taking into consideration the above, as well as the observation that the methylene protons H_2-12 were magnetically equivalent in **2** and resonated at different sites in **3**, the difference between them could only be attributed to a change in the relative configuration at C-13.

In an effort to investigate the configuration at C-13 for compounds **2** and **3**, conformational analysis and molecular dynamics simulations (MD) were applied. Theoretical studies performed on **2** and **3**, assuming arbitrarily *S** and *R** chirality of C-13, respectively, were combined with the observed NOE data aiming to associate the two proposed structures with the corresponding ^{1}H NMR spectra. Comparison of the NOESY spectra of the two compounds showed that the only differences between them were the NOE enhancement of H-3/H_2-12, apparent only in the spectrum where H_2-12 are magnetically equivalent (metabolite **2**) and the NOE correlation of H-3/H-11b in the spectrum where H_2-12 resonate at distinct sites (metabolite **3**).

Monte Carlo conformational search revealed two main conformations of the bicyclic system (A and B), differing in the dihedral angle R (C-8–C-7–C-6–C-5). Representative low energy conformers of the two conformations are depicted in Figure. 2. Conformation A, which emerged as the most energetically favourable and by far the most populated (143 out of 148 derived conformers for the 13*S**-epimer and 170 in an assembly of 172 for the 13*R**-epimer), adopted a value of approximately 60° for the dihedral angle R, leading to an envelope conformation for the six-membered ring, where C-7 was oriented towards the α-face and a distorted envelope conformation for the five-membered ring, with C-6 positioned below the ring plane. Conformation B, which was less energetically favourable and less populated, adopted a value of approximately 170° for the torsion angle R (bond C-7–C-8 was almost parallel to bond C-5–C-6), setting the six-membered ring in a distorted envelope configuration, with C-7 placed in β-orientation and the five-membered ring to an envelope conformation, with C-6 positioned above the ring plane. Both conformations justified the arrangement of H-10 and H_3-17 below the plane of the adjacent ring, as confirmed experimentally by their NOE interactions with H-18. Furthermore, conformation A was consistent with the observed NOE correlations of H-5β/H-8β and H-4α/H_3-20, while there was no NOE signal to support conformation B of the ring system.

The conformational features of the alkyl chain were more systematically explored by applying grid scan search around the two dihedral angles τ1 (C-2–C-3–C-10–C-11) and τ2 (C-3–C-10–C-11–C-12) of the favourable conformation A. The potential energy contour plots as a function of the dihedral angles τ1 and τ2 for the two epimers at C-13 are shown in Figure 3(i). Variation of the torsion angles in a stepwise manner resulted in six distinct areas and A1–A6 indicate the corresponding conformational local minima depicted in Figure 3(ii). The torsion angles of the conformers are reported in Table S1 (supplementary data). Inspection of the energy maps revealed that values of the dihedral angle τ1 in the range of 45–165° were favoured (conformers $A1_S$-$A5_S$ of **2** and $A1_R$-$A5_R$ of **3**), placing H_3-17 and H-10 below the plane of the adjacent five-membered ring, while values greater than 180° turned H_3-17 and H-10 towards H-3 ($A6_S$ of **2** and $A6_R$ of **3**), which was energetically unfavourable and contradicted the NOE data. The dihedral angle τ2 could adopt a *gauche*(−) configuration ($A1_S$ of **2** and $A1_R$ of **3**), a *gauche*(+) configuration ($A3_S$ of **2** and $A3_R$ of **3**) or a *trans* configuration ($A2_S$, $A4_S$ and $A5_S$ of **2** and $A2_R$, $A4_R$ and $A5_R$ of **3**). The first two arrangements permitted the dipolar interaction between H-3/H_2-12, while the latter one supported the NOE signal between H-3/H-11b. A thorough study of the energy maps denoted a prevalence for the *gauche*(−) configuration of the dihedral angle τ2 for the 13*S**-epimer, since conformer $A1_S$ emerged as the global minimum. Accordingly, a preference for the *trans* configuration was observed for the 13*R**-epimer, as $A4_R$ was the lowest energy conformer. Furthermore, as it could be concluded from the energy plots, the *gauche*(-) and the *trans* configurations energy areas surrounded by the lowest isoenergetic curve included a respectively greater number of conformers. Consequently, grid scan analysis results supported the 13*S** chirality for metabolite **2** and the 13*R** chirality for metabolite **3**.

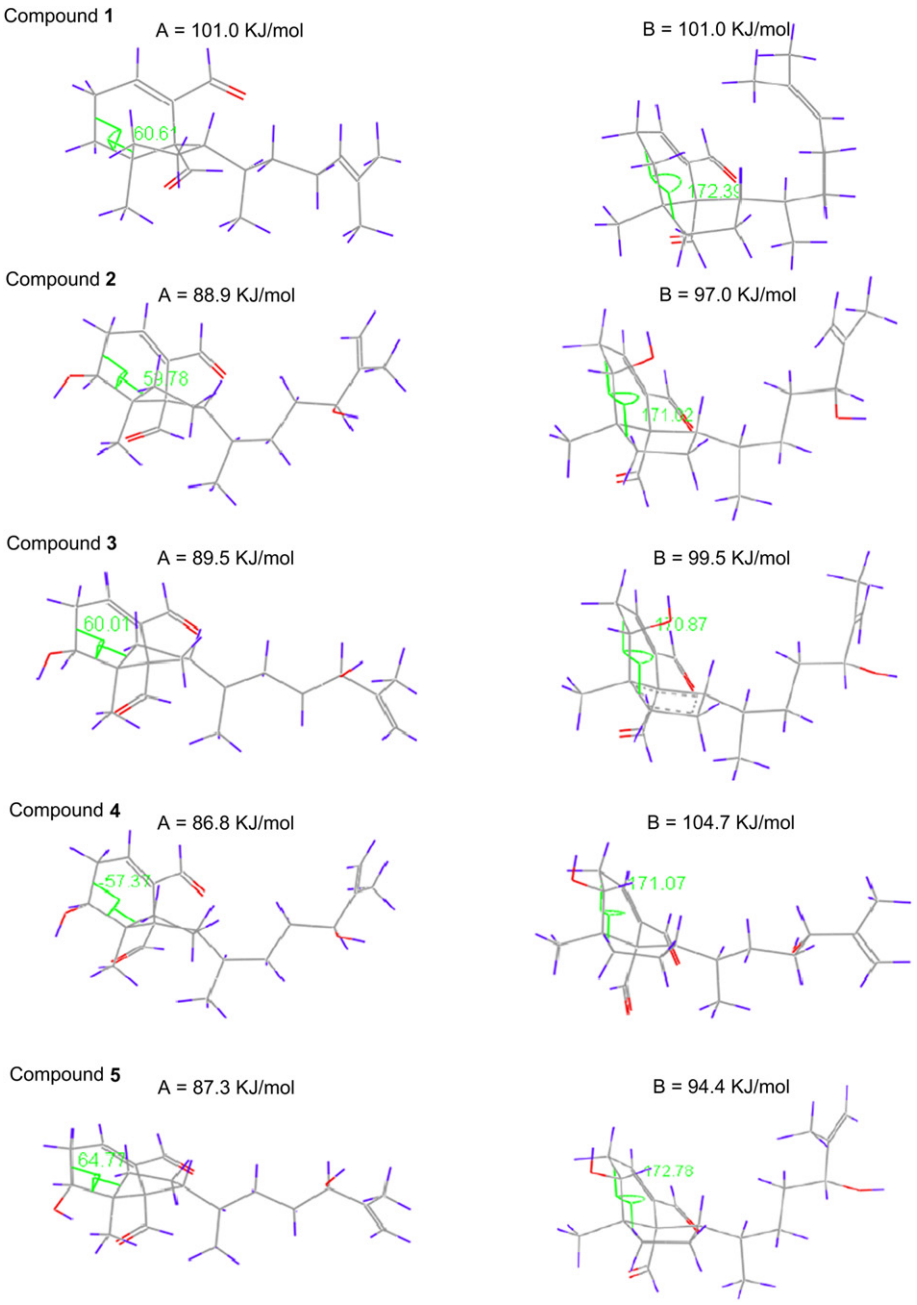

Figure 2. Representative low energy conformers for compounds **1**–**5**, indicating the two conformations (A and B) of the bicyclic system. The associated energy values are also noted.

In order to further validate the above results, unconstrained MD simulations were applied to all derived conformational minima. Thus, in an effort to extract dynamic information about the evolution of the two systems, different initial conditions were applied for a long period of simulation time. Favourable conformers $A1_S$ and $A2_S$ of **2**, as well as $A1_R$ and $A2_R$ of **3**, adopting a *gauche*(−) or a *trans* orientation for H_2-12 were found to be dynamically stable (Fig. S1, supplementary data). Moreover, time evolution for the favourable conformers of compound **2** revealed a preference for the *gauche*(−) configuration (50–60% of conformations), while as far as compound **3** is concerned, inspection of the trajectories confirmed a preference for the *trans* configuration of the dihedral angle τ2 (50–60% of conformations).

Unconstrained MD simulations were also applied to the favourable conformers of **2** and **3**, derived from the Monte Carlo analysis, adopting conformation B of the bicyclic system. Surprisingly, a conversion of the ring system from B to A conformation was observed even from the equilibration time (for **2**) or within the first 2 ns of the production period (for **3**), denoting the main occurrence of conformation A. Dihedral angle τ2 values distribution along the last period of simulation where the potential energy fluctuation was negligible further confirmed the preference for the *trans* configuration associated with the R^* chirality and the *gauche* configuration associated with the S^* chirality of C-13 (Fig. S2, supplementary data).

Concluding, in accordance with grid scan analysis, MD simulations results validated the assumption that the S^* chirality of C-13 correlated with the ^{1}H NMR spectrum where H_2-12 were magnetically equivalent corresponding to compound **2**, while the R^* chirality of C-13 correlated with the ^{1}H NMR spectrum where H_2-12 resonate at distinct sites and corresponded to compound **3**.

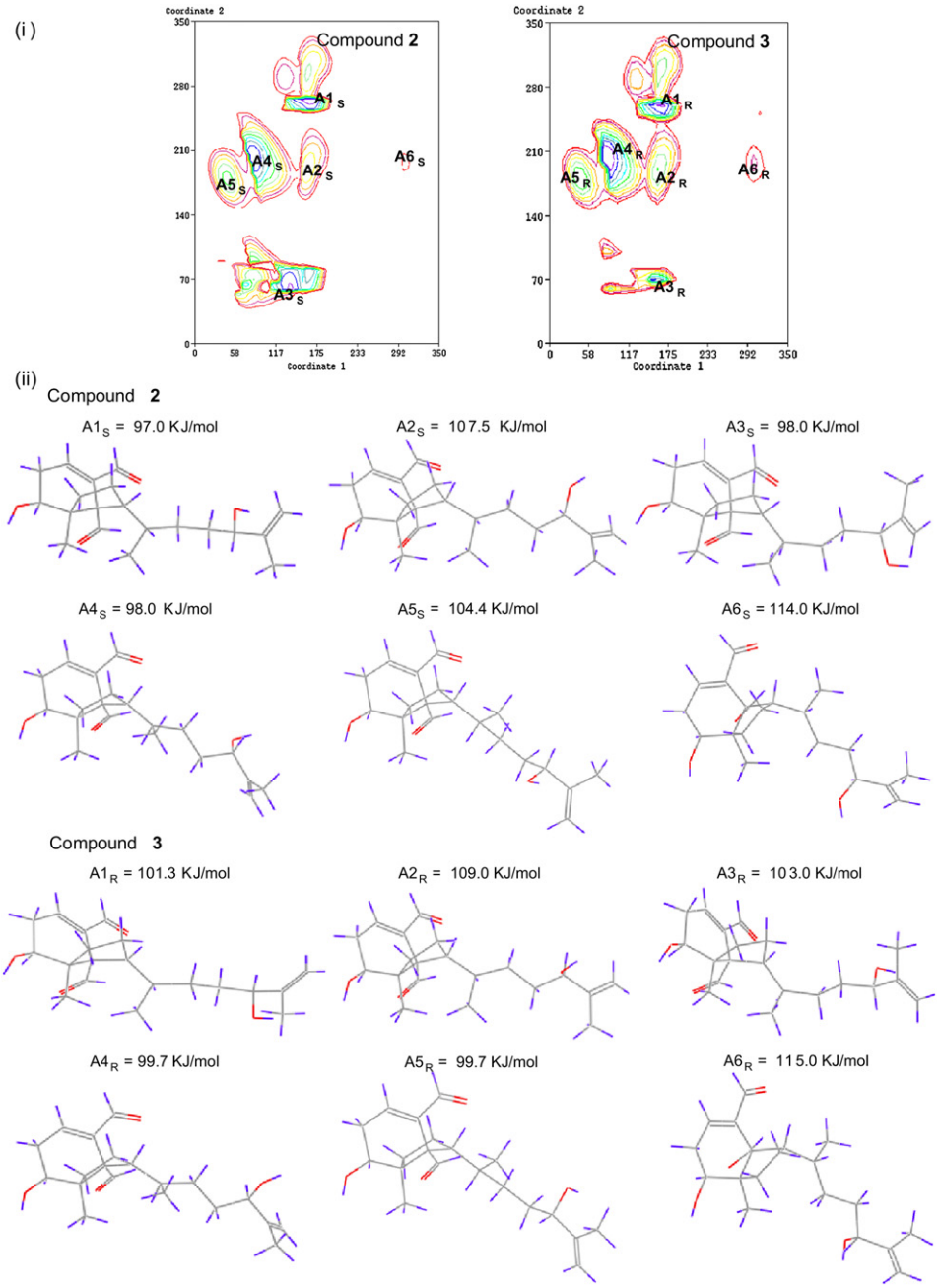

Figure 3. (i) Contour maps generated for conformation A of compounds **2** and **3** by rotating around dihedral angles τ1 and τ2 in increments of 10°. The contour levels, which are up to 20 KJ/mol higher than the global minimum, are plotted with a step of 2 KJ/mol. (ii) Representative conformational minima for compounds **2** and **3** extracted from grid scan search.

Compounds **4** and **5**, obtained both as colourless oils, were isolated by HPLC as two distinct peaks with a difference of 0.85 min in their elution times and displayed the molecular formula of $C_{20}H_{30}O_4$, according to the HR-FABMS data (*m*/*z* 334.2153 $[M]^+$ for **4** and *m*/*z* 334.2159 $[M]^+$ for **5**). Their ^1H NMR spectra contained signals for two methyls on quaternary carbons (δ 1.05 and 1.77), one methyl on a tertiary carbon (δ 0.98), two oxygenated methines (δ 3.77 and 4.32), an exomethylene group (δ 4.85 and 4.98), an olefinic proton of a trisubstituted double bond (δ 6.83), and two aldehyde methines (δ 9.34 and 9.91). Interpretation of their spectroscopic data (Tables 1 and 2) showed a high degree of similarity with metabolites **2** and **3** and analysis of the homonuclear and heteronuclear correlations observed in their respective HSQC, HMBC and COSY spectra indicated that **4** and **5** were the epimers of **2** and **3** at C-7. Again, the only obvious difference between compounds **4** and **5** was that the methylene protons H_2-12 were magnetically equivalent in **4**, both resonating at δ 1.75 ppm, while in **5** they resonated at δ 1.72 and 1.85 ppm.

The relative configuration of the stereogenic centres in compounds **4** and **5** was determined on the basis of the key correlations observed in their respective NOESY spectra. In accordance with metabolites **1**–**3**, the relative configuration at C-2, C-3, C-6 and C-10 was determined as 2*R**,3*S**,6*R**,10*R** due to the NOE enhancements of H-3/H-4β, H-4α/H_3-17, H-10/H-18, H_3-17/H-18 and H-18/H_3-20, whereas the relative configuration at C-7 was assigned as *R** based on the NOE cross-peaks between H-7 and both H-3 and H-4β. Based on the above and in conjunction with the fact that the methylene protons H_2-12 were magnetically equivalent in **4** and resonated at

different sites in **5**, it was assumed that the difference between them was due to a change in the relative configuration at C-13, as in the case of compounds **2** and **3**.

Following the same rationale as in the case of metabolites **2** and **3**, *S** and *R** chirality of C-13 was arbitrarily assumed for **4** and **5**, respectively. The same theoretical analyses were applied in order to verify the correspondence of the ^{1}H NMR spectra to the proposed relative configuration at C-13. Monte Carlo conformational search revealed, as in the previous case, the existence of two ring system conformations, namely A and B, arranging the ring system in a similar way as the one described for **2** and **3** (Fig. 2). Conformation A, which emerged energetically more favourable and more populated (314 out of 318 derived conformers for the 13*S**-epimer and 291 in an assembly of 315 for the 13*R**-epimer), was consistent with the NOE interactions of H-5β/H-8β, H-4α/H_3-20 and H-7/H_3-20. Conformation B emerged by far less populated and energetically less favourable, but could not be overlooked since it was consistent with the observed weak NOE enhancements of H-3/H-7, H-4β/H-7 and H-5β/H-7.

Potential energy contour plots derived from systematic variation around dihedral angles τ1 and τ2 for the representative low energy A conformers of **4** and **5** emerged similar to the corresponding ones for **2** and **3**, presenting a global minimum for the *gauche*(−) configuration of the dihedral angle τ2 in the case of the 13*S**-epimer, while the 13*R**-epimer seemed to favour the *trans* configuration, positioning the H_2-12 away from ring proton H-3 (Fig. S3, Supplementary data). Besides, as in the case of **2** and **3**, the *gauche*(−) and the *trans* configurations energy areas bounded by the lowest isoenergetic curves were found to encompass a respectively greater number of conformers. Since comparison of the NOESY spectra of **4** and **5** revealed that the only differences between them were the NOE enhancement of H-3/H_2-12, apparent only in the spectrum where H_2-12 are magnetically equivalent (metabolite **4**) and the NOE correlation of H-3/H-11b in the spectrum where H_2-12 resonate at distinct sites (metabolite **5**), grid scan results suggested that **4** and **5** were associated with the *S** and *R** chirality of C-13, respectively. Favourable conformers were subjected to unconstrained MD simulations and the resulting τ2 values distribution was in agreement with the previous conclusion (Fig. S4, Supplementary data).

Favourable conformers adopting conformation B were also subjected to MD simulations. No specific preference regarding H_2-12 orientation could be derived, implying a greater flexibility of the alkyl chain associated with conformation B of the bicyclic system. However, it has to be noted that in contrast with compounds **2** and **3**, conformation B of the ring system for **4** and **5** was retained at least for the longest period of the simulation time (Fig. S5, Supplementary data). Based on this observation, it could be deduced that the energy barrier for the interconversion between the two conformations (A and B) should have a lower value in the case of **4** and **5**, as compared with that of **2** and **3**, but this would have to be confirmed by applying more thorough theoretical calculations.

Compounds **6** and **7**, isolated both as colourless oils, displayed molecular ion peaks at *m*/*z* 318 (EIMS), corresponding to $C_{20}H_{30}O_3$. The spectroscopic characteristics of **6** and **7** showed a high degree of similarity with those of metabolites **1**–**5**. Specifically, the ^{1}H NMR spectra of both compounds indicated the presence of three methyls on quaternary carbons (δ 1.16, 1.58 and 1.66 for **6** and 1.05, 1.57 and 1.66 for **7**), one methyl on a tertiary carbon (δ 1.05 for **6** and 0.97 for **7**), an oxygenated methine (δ 3.82 for **6** and 3.77 for **7**), two olefinic methines (δ 5.09 and 6.72 for **6** and 5.06 and 6.81 for **7**), and two aldehyde groups (δ 9.26 and 9.97 for **6** and 9.33 and 9.94 for **7**). In agreement with their molecular formula, it was obvious that **6** and **7** were the two epimeric 7-hydroxy derivatives of **1**. Even though compounds **6** and **7** proved to be unstable and degraded soon after their isolation, thus not allowing for the measurement of ^{13}C NMR spectra or the complete assignment of ^{1}H NMR chemical shifts, the high degree of similarity in the chemical shifts and coupling constants of H-3, H-7, H-9, H_3-17, H-18, H-19 and H_3-20 for **2**, **3** and **6**, as well as for **4**, **5** and **7** was adequate evidence for the safe structure elucidation of **6** and **7**.

In order to investigate the conformation of the ring system when the 7-OH functionality is lacking, **1** was also subjected to Monte Carlo conformational analysis and MD simulations. Conformations A and B emerged isoenergetic (Fig. 2). Furthermore, MD simulations revealed the fast interchange between the two conformations, since the distribution of the torsion angle R between the two rings showed their equipotent existence. Since MD simulations were performed at ambient temperature, this was an indication of the very low energy barrier needed to be overcome for the interconversion of the two conformations (Fig. S6, Supplementary data).

To the best of our knowledge, this is only the second report on the isolation of natural products featuring the 2,6-*cyclo*-xenicane ring system. Previously, the 7-hydroxy and 7-acetoxy derivatives of 2,6-*cyclo*-1(19),13-xenicadiena-18,19-dial were isolated from an Australian collection of the brown alga *D. dichotoma*.[3] However, only key NMR spectroscopic characteristics were assigned and their relative stereochemistry was not determined. Even though metabolites **6** and **7** have the same planar structure with the reported metabolite, their spectroscopic data are not the same, suggesting that the relative configuration of those compounds was different from the one depicted for **6** and **7**.

3. Experimental

3.1. General experimental procedures

Optical rotations were measured on a Perkin–Elmer model 341 polarimeter with a 1 dm cell. UV spectra were obtained on a Shimadzu UV-160A spectrophotometer. IR spectra were obtained on a Bruker Tensor 27 spectrometer. NMR spectra were recorded on Bruker DRX 400 and Varian 600 spectrometers. Chemical shifts are given on a δ (ppm) scale using TMS as internal standard. The 2D experiments (HSQC, HMBC, COSY, NOESY) were performed using standard Varian pulse sequences. High resolution FAB mass spectra data were provided by the University of Notre Dame, Department of Chemistry and Biochemistry, Notre Dame, Indiana, USA. Low resolution EI mass spectra were measured on a Hewlett Packard 5973 mass spectrometer. Low resolution CI mass spectra were measured in positive mode on a Thermo Electron Corporation DSQ mass spectrometer using a Direct-Exposure Probe and methane as the CI reagent gas. Column chromatography separations were performed using Kieselgel 60 (Merck). HPLC separations were conducted using a CECIL 1100 Series liquid chromatography pump equipped with a GBC LC-1240 refractive index detector, using the following columns: (i) Spherisorb S10W (Phase Sep, 25 cm×10 mm), (ii) Econoshpere Silica 10u (Grace, 25 cm×10 mm), (iii) Kromasil 100 SIL (MZ-Analysentechnik, 25 cm×8 mm), and (iv) Chiralcel OD 10 μm (Daicel Chemical Industries Ltd., 25 cm×10 mm). TLC were performed with Kieselgel 60 F_{254} (Merck aluminium support plates) and spots were detected after spraying with 15% H_2SO_4 in MeOH reagent and heating at 100 °C for 1 min. The lyophilisation was carried out in a Freezone 4.5 freeze dry system (Labconco).

3.2. Plant material

D. spiralis was collected by hand in Elafonissos island, south of Peloponnese, Greece, at a depth of 0.1–1 m in April of 2004, while *D. fasciola* was collected by hand at Cap Zebib, in the north coasts of Tunisia, at a depth of 0.1–2 m in July of 2006. Voucher specimens of the two algae are kept at the Herbarium of the Department of Pharmacognosy and Chemistry of Natural Products, University of

Athens (ATPH/MO/159) and at the Laboratory of the National Institute of Marine Sciences and Technologies (CZ100706-1), respectively.

3.3. Extraction and isolation

Specimens of the freeze-dried alga *D. spiralis* (272 g) were exhaustively extracted with CH_2Cl_2 and subsequently with MeOH at room temperature. Evaporation of the solvents in vacuo afforded two dark green oily residues. The CH_2Cl_2 residue (9.2 g) was subjected to vacuum column chromatography on silica gel, using *c*-hexane with increasing amounts of EtOAc, followed by EtOAc with increasing amounts of MeOH as the mobile phase, to afford fifteen fractions (A1–A15). Fraction A3 (20% EtOAc in *c*-hexane, 1.17 g) was further fractionated by gravity column chromatography on silica gel, using *c*-hexane with increasing amounts of EtOAc as the mobile phase, to yield twenty-one fractions (A3a–A3u). Fraction A3i (2% EtOAc, 81.7 mg) was purified by normal phase HPLC, using *c*-hexane/EtOAc (95:5) as eluant, to yield pachylactone (0.8 mg). Fraction A3l (10% EtOAc, 81.9 mg) was subjected to gravity column chromatography on silica gel, using *c*-hexane with increasing amounts of EtOAc as the mobile phase, to yield ten fractions (A3l1–A3l10). Fractions A3l9 (8% EtOAc, 3.3 mg) and A3 m (20% EtOAc, 20.1 mg) were purified by normal phase HPLC, using *c*-hexane/EtOAc (90:10) as eluant, to afford fucosterol (2.7 mg). Fraction A4 (30% EtOAc in *c*-hexane, 3.58 g) was further fractionated by vacuum column chromatography on silica gel, using *c*-hexane with increasing amounts of EtOAc, followed by EtOAc with increasing amounts of MeOH as the mobile phase, to afford nine fractions (A4a–A4i). Fraction A4c (20% EtOAc in *c*-hexane, 812.3 mg) was subjected to gravity column chromatography on silica gel, using *c*-hexane with increasing amounts of EtOAc, followed by EtOAc with increasing amounts of MeOH as the mobile phase, to yield twenty-three fractions (A4c1–A4c23). Fractions A4c2 (1% EtOAc in *c*-hexane, 174.3 mg) and A4c3 (1% EtOAc in *c*-hexane, 129.8 mg) were separately purified by normal phase HPLC, using *n*-hexane/EtOAc (97:3) and subsequently *n*-hexane/*i*-propanol (99.5:0.5) as eluant, to afford obscuronatin (1.5 mg). Fractions A4c10 (2% EtOAc in *c*-hexane, 17.0 mg), A4c11 (3% EtOAc in *c*-hexane, 10.8 mg), A4c12 (5% EtOAc in *c*-hexane, 18.7 mg), A4c13 (7% EtOAc in *c*-hexane, 47.0 mg), and A4c15 (12% EtOAc in *c*-hexane, 138.5 mg) were separately and repeatedly purified by normal phase HPLC, using *c*-hexane/EtOAc (90:10) as eluant, to afford neodictyolactone (1.4 mg), acetyldictyolal (7.0 mg), *trans*-phytol (7.4 mg), fucosterol (0.6 mg), and compound **1** (1.1 mg). Fraction A8 (70% EtOAc in *c*-hexane, 177.9 mg) was further fractionated by gravity column chromatography on silica gel, using *c*-hexane with increasing amounts of EtOAc as the mobile phase, to yield ten fractions (A8a–A8j), among which A8e (40% EtOAc, 69.8 mg) was identified as all-*E*-(3*S*,5*R*,6*S*,3′*S*,5′*R*,6′*R*)-fucoxanthin. The MeOH residue (32.8 g) was subjected to vacuum column chromatography on silica gel, using *c*-hexane with increasing amounts of EtOAc, followed by EtOAc with increasing amounts of MeOH as the mobile phase, to afford fourteen fractions (B1–B14). Fraction B3 (20% EtOAc, 361.0 mg) was repeatedly purified by normal phase HPLC, using *c*-hexane/EtOAc (90:10) and subsequently *n*-hexane/*i*-propanol (83:17) as eluant, to yield acetyldictyolal (4.7 mg), neodictyolactone (1.0 mg), *trans*-phytol (0.8 mg), and fucosterol (2.7 mg).

Specimens of the air-dried alga *D. fasciola* (11 g) were exhaustively extracted with CH_2Cl_2/MeOH (1:1) at room temperature. Evaporation of the solvent in vacuo afforded a green oily residue (617 mg) that was subjected to gravity column chromatography on silica gel, using *c*-hexane with increasing amounts of EtOAc, followed by EtOAc with increasing amounts of MeOH as the mobile phase, to afford nineteen fractions (I-XIX). Fraction V (5% EtOAc in *c*-hexane, 12.7 mg) was subjected to normal phase HPLC, using *c*-hexane/EtOAc (95:5) as eluant, to afford 18-hydroxy-2,7-dolabelladiene (4.9 mg) and neodictyolactone (2.4 mg). Fraction VI (5% EtOAc in *c*-hexane, 14.7 mg) was subjected to normal phase HPLC, using *c*-hexane/EtOAc (95:5) as eluant, to afford acetyldictyolal (2.1 mg). Fraction VIII (10% EtOAc in *c*-hexane, 19.4 mg) was identified as fucosterol. Fraction IX (10% EtOAc in *c*-hexane, 55.4 mg) was subjected to normal phase HPLC, using *c*-hexane/EtOAc (88:12) as eluant, to afford dictyol E (19.4 mg) and sanadaol (1.0 mg). Fraction XII (25% EtOAc in *c*-hexane, 45.0 mg) was subjected to normal phase HPLC, using *c*-hexane/EtOAc (80:20) as eluant, to afford dictyol C (5.3 mg). Fraction XIII (35% EtOAc in *c*-hexane, 20.0 mg) was subjected repeatedly to normal phase HPLC, using *c*-hexane/EtOAc (70:30 and 65:35) as eluant, to yield **4** (0.4 mg), **5** (0.4 mg), and **7** (0.2 mg). Fraction XIV (40% EtOAc in *c*-hexane, 25.0 mg) was subjected repeatedly to normal phase HPLC, using *c*-hexane/EtOAc (70:30 and 65:35) as eluant, to yield **2** (0.4 mg), **3** (0.4 mg), and **6** (0.3 mg).

3.3.1. (2R,3S*,6R*,10R*)-2,6-cyclo-1(9),13-Xenicadiene-18,19-dial (**1**).* Colourless oil; $[\alpha]_D^{20}$ +12 (*c* 0.067, $CHCl_3$); UV ($CHCl_3$) λ_{max} (log ε) 229.5 (3.29) nm; IR (thin film) ν_{max} 2930, 1717, 1698, 1276 cm^{-1}; ^1H NMR data, see Table 1; ^{13}C NMR data, see Table 2; EIMS 70 eV *m*/*z* (rel int. %) 302 (32), 284 (77), 269 (32), 251 (21), 241 (35), 219 (42), 213 (80), 201 (35), 185 (49), 173 (100), 161 (28), 151 (60), 145 (48), 131 (51), 119 (27), 109 (69), 91 (71), 79 (42), 69 (76), 55 (50); HR-FABMS *m*/*z* 303.2340 $[M+H]^+$ (calcd for $C_{20}H_{31}O_2$, 303.2324).

3.3.2. (2R,3S*,6R*,7S*,10R*,13S*)-7,13-Dihydroxy-2,6-cyclo-1(9),14-xenicadiene-18,19-dial (**2**).* Colourless oil; $[\alpha]_D^{20}$ −21 (*c* 0.033, $CHCl_3$); UV ($CHCl_3$) λ_{max} (log ε) 228.5 (2.97) nm; IR (thin film) ν_{max} 3358, 3331, 2936, 1725, 1693, 1259 cm^{-1}; ^1H NMR data, see Table 1; ^{13}C NMR data, see Table 2; PCIMS (CH_4) *m*/*z* (rel int. %) 335 (1), 317 (8), 299 (28), 281 (43), 271 (56), 251 (65), 235 (34), 225 (18), 213 (26), 197 (36), 185 (47), 171 (24), 161 (40), 145 (23), 131 (24), 121 (15), 109 (100), 91 (18), 85 (46), 69 (14), 55 (17); HR-FABMS *m*/*z* 334.2171 $[M]^+$ (calcd for $C_{20}H_{30}O_4$, 334.2144).

3.3.3. (2R,3S*,6R*,7S*,10R*,13R*)-7,13-Dihydroxy-2,6-cyclo-1(9),14-xenicadiene-18,19-dial (**3**).* Colourless oil; $[\alpha]_D^{20}$ −18 (*c* 0.033, $CHCl_3$); UV ($CHCl_3$) λ_{max} (log ε) 229.0 (2.93) nm; IR (thin film) ν_{max} 3351, 3339, 2933, 1721, 1697, 1263 cm^{-1}; ^1H NMR data, see Table 1; ^{13}C NMR data, see Table 2; PCIMS (CH_4) *m*/*z* (rel int. %) 335 (1), 317 (11), 299 (25), 281 (37), 271 (35), 251 (40), 235 (41), 225 (13), 213 (18), 197 (25), 185 (36), 171 (17), 161 (32), 145 (19), 131 (19), 121 (12), 109 (100), 91 (10), 85 (25), 69 (7), 55 (7); HR-FABMS *m*/*z* 334.2163 $[M]^+$ (calcd for $C_{20}H_{30}O_4$, 334.2144).

3.3.4. (2R,3S*,6R*,7R*,10R*,13S*)-7,13-Dihydroxy-2,6-cyclo-1(9),14-xenicadiene-18,19-dial (**4**).* Colourless oil; $[\alpha]_D^{20}$ −27 (*c* 0.033, $CHCl_3$); UV ($CHCl_3$) λ_{max} (log ε) 228.5 (2.91) nm; IR (thin film) ν_{max} 3348, 3337, 2928, 1719, 1699, 1267 cm^{-1}; ^1H NMR data, see Table 1; ^{13}C NMR data, see Table 2; PCIMS (CH_4) *m*/*z* (rel int. %) 335 (4), 317 (8), 299 (57), 281 (72), 271 (23), 251 (60), 235 (41), 225 (33), 211 (50), 197 (41), 185 (24), 171 (22), 157 (32), 145 (27), 131 (29), 119 (22), 109 (100), 91 (27), 85 (24), 69 (19), 55 (20); HR-FABMS *m*/*z* 334.2153 $[M]^+$ (calcd for $C_{20}H_{30}O_4$, 334.2144).

3.3.5. (2R,3S*,6R*,7R*,10R*,13R*)-7,13-Dihydroxy-2,6-cyclo-1(9),14-xenicadiene-18,19-dial (**5**).* Colourless oil; $[\alpha]_D^{20}$ −39 (*c* 0.033, $CHCl_3$); UV ($CHCl_3$) λ_{max} (log ε) 229.5 (3.01) nm; IR (thin film) ν_{max} 3352, 3327, 2929, 1717, 1689, 1262 cm^{-1}; ^1H NMR data, see Table 1; ^{13}C NMR data, see Table 2; PCIMS (CH_4) *m*/*z* (rel int. %) 335 (3), 317 (9), 299 (59), 281 (53), 271 (31), 251 (68), 235 (38), 225 (30), 211 (36), 197 (31), 185 (39), 171 (27), 157 (26), 145 (24), 131 (30), 119

(12), 109 (100), 91 (21), 85 (57), 69 (22), 55 (17); HR-FABMS *m*/*z* 334.2159 $[M]^+$ (calcd for $C_{20}H_{30}O_4$, 334.2144).

3.3.6. (2R,3S*,6R*,7S*,10R*)-7-Hydroxy-2,6-cyclo-1(9),13-xenicadiene-18,19-dial (**6**).* Colourless oil; ^{1}H NMR ($CDCl_3$) δ 9.97 (1H, s, H-18), 9.26 (1H, s, H-19), 6.72 (1H, dd, *J*=5.7, 2.2 Hz, H-9), 5.09 (1H, m, H-13), 3.82 (1H, dt, *J*=9.8, 5.7 Hz, H-7), 2.67 (1H, dt, *J*=19.6, 5.7 Hz, H-8a), 2.56 (1H, m, H-10), 2.36 (1H, ddd, *J*=19.6, 9.8, 2.2 Hz, H-8b), 2.10 (1H, m, H-3), 1.66 (3H, s, H-15), 1.58 (3H, s, H-16), 1.16 (3H, s, H-20), 1.05 (3H, d, *J*=6.7 Hz, H-17); EIMS 70 eV *m*/*z* (rel int. %) 318 (8), 300 (47), 282 (43), 235 (29), 218 (11), 200 (13), 161 (23), 144 (26), 131 (32), 119 (9), 109 (100), 91 (19), 79 (46), 69 (21), 55 (42).

3.3.7. (2R,3S*,6R*,7R*,10R*)-7-Hydroxy-2,6-cyclo-1(9),13-xenicadiene-18,19-dial (**7**).* Colourless oil; ^{1}H NMR ($CDCl_3$) δ 9.94 (1H, s, H-18), 9.33 (1H, s, H-19), 6.81 (1H, dd, *J*=4.5, 3.2 Hz, H-9), 5.06 (1H, m, H-13), 3.77 (1H, dt, *J*=8.7, 4.5 Hz, H-7), 2.71 (1H, ddd, *J*=20.1, 4.5, 3.2 Hz, H-8a), 2.56 (1H, dt, *J*=20.1, 4.5 Hz, H-8b), 2.50 (1H. m, H-10), 2.10 (1H, m, H-3), 1.66 (3H, s, H-15), 1.57 (3H, s, H-16), 1.05 (3H, s, H-20), 0.97 (3H, d, *J*=6.7 Hz, H-17); EIMS 70 eV *m*/*z* (rel int. %) 318 (6), 300 (45), 282 (49), 235 (26), 218 (14), 200 (15), 161 (27), 144 (21), 131 (35), 119 (12), 109 (100), 91 (23), 79 (51), 69 (26), 55 (49).

3.4. Molecular modelling and conformational search

Conformational analysis studies were performed using MacroModel 9.5 (Schrödinger Inc.) s/w. The MM2* force field was applied for the potential energy calculations and all studies were run using a dielectric constant ε=1 to simulate $CDCl_3$ environment. Monte Carlo searches were performed using MCMM/LMOD routine. PRCG algorithm was used for energy optimisation with 0.001 convergence threshold. 5000 steps were run and the derived conformers were clustered by atomic rms in five families, the lowest energy members of which were chosen for further analyses. Grid scan searches were performed using Maestro Dihedral Scan applying the same force field and keeping the same dielectric constant. The initial structures were subjected to a systematic variation around torsion angles τ1 and τ2 from 0° to 360° applying a torsion step of 10°. The derived conformations were optimised by applying PRCG algorithm with an energy gradient tolerance of 0.001 Kcal/mol Å as convergence criterion. Molecular Dynamics simulations were run using Stochastic Dynamics method. The simulation temperature was 300 K in order to simulate the spectroscopic experimental conditions. Local minima derived from Grid Scan analyses were further optimised by applying PRCG algorithm. Then, a 2 ns equilibrium run was performed, followed by a 20 ns simulation. The time step was set to 1 fs and 5000 samples were collected. Potential energy calculations were performed using MM2* force field in $CDCl_3$ environment. All critical dihedral angles and interatomic distances were monitored during the simulation. Visualisation of the 3D structures has been enabled by the use of Accelrys DS Visualiser s/w.

Acknowledgements

Financial support from the Greek General Secretariat for Research and Technology and the Tunisian Ministry of Higher Education, Scientific Research and Technology (39/TG/05) in the framework of a Joint Research and Technology Programme between Greece and Tunisia (2005–2007) is gratefully acknowledged. Thanks are also due to M. El Bour and H. Langar for their assistance in earlier stages of this work.

Supplementary data

Supplementary data associated with this article can be found in the online version, at doi:10.1016/j.tet.2009.10.081.

References and notes

1. Blunt, J. W.; Copp, B. R.; Hu, W.-P.; Munro, M. H. G.; Northcote, P. T.; Prinsep, M. R. *Nat. Prod. Rep.* **2009**, *26*, 170–244 and earlier reviews in this series.
2. MarinLit database, Department of Chemistry, University of Canterbury: http://www.chem.canterbury.ac.nz/marinlit/marinlit.shtml.
3. Blount, J. F.; Dunlop, R. W.; Erickson, K. L.; Wells, R. J. *Aust. J. Chem.* **1982**, *35*, 145–163.
4. Enoki, N.; Ishida, R.; Matsumoto, T. *Chem. Lett.* **1982**, 1749–1752.
5. Ishitsuka, M.; Kusumi, T.; Tanaka, J.; Chihara, M.; Kakisawa, H. *Chem. Lett.* **1984**, 151–154.
6. Ishitsuka, M.; Kusumi, T.; Kakisawa, H.; Kawakami, Y.; Nagai, Y.; Sato, T. *Tetrahedron Lett.* **1983**, *24*, 5117–5120.
7. Kashman, Y.; Groweiss. *J. Org. Chem.* **1980**, *45*, 3814–3824.
8. Kodama, M.; Okumura, K.; Kobayashi, Y.; Tsunoda, T.; Ito, S. *Tetrahedron Lett.* **1984**, *25*, 5781–5784.
9. Ishitsuka, M.; Kusumi, T.; Kakisawa, H.; Kawakami, Y.; Nagai, Y.; Sato, T. *Tetrahedron Lett.* **1986**, *27*, 2639–2642.
10. Sims, J. J.; Pettus, J. A., Jr. *Phytochemistry* **1976**, *15*, 1076–1077.
11. Brown, G. D. *Phytochemistry* **1994**, *36*, 1553–1554.
12. Nes, W. R.; Castle, M.; McClanahan, J. L.; Settine, J. M. *Steroids* **1966**, *8*, 655–657.
13. Frost, D. J.; Ward, J. P. *Tetrahedron Lett.* **1968**, *9*, 3779–3782.
14. Haugan, J. A.; Liaaen-Jensen, S. *Phytochemistry* **1992**, *31*, 1359–1361.
15. Haugan, J. A.; Liaaen-Jensen, S. *Tetrahedron Lett.* **1994**, *35*, 2245–2248.
16. Danise, B.; Minale, L.; Riccio, R.; Amico, V.; Oriente, G.; Piattelli, M.; Tringali, C.; Fattorusso, E.; Magno, S.; Mayol, L. *Experientia* **1977**, *33*, 413–415.
17. Ishitsuka, M.; Kusumi, T.; Kakisawa, H. *Tetrahedron Lett.* **1982**, *23*, 3179–3180.
18. König, G. M.; Wright, A. D.; Sticher, O. *Phytochemistry* **1991**, *30*, 3679–3682.